UNIVERSITÀ DEGLI STUDI DI PADOVA

Dipartimento di Fisica e Astronomia "Galileo Galilei"

Corso di Laurea in Fisica

Tesi di Laurea

Study of a cosmic ray detector based on drift tubes

Relatore

Dr. Paolo Checchia

Laureando

Carlo Sgorlon Gaiatto

Anno Accademico 2020/2021

Abstract

Muon tomography is a promising imaging technique for the inspection of dry storage casks (DSC) for spent nuclear fuel. Recently, it has been proposed to implement drift tube detectors to control the content of DSCs. The main objective of this thesis is the analysis of the radial and longitudinal spatial resolution of a drift tube detector. The muon tomography demonstrator installed at Legnaro National Laboratories, consisting of two CMS chambers, has been used to reconstruct the muon tracks and to provide a trigger system for the drift tube. Furthermore, a simulation of the muon flux has been performed to test the optimal position of CMS superlayers with respect to detectors, obtained by joining several layers of drift tubes of the type described in this study, placed around a CASTOR®-V cask.

Contents

Introduction

1.1 Cosmic rays

Cosmic rays are high-energy particles arriving from outer space at nearly the speed of light. They originate from different astrophysical sources, such as the Sun, supernovae and distant galaxies, although there is still scientific debate about this. Primary cosmic rays consists predominantly of protons (89%), alpha particles (8%) and heavier nuclei, even if the relative composition depends on the kinetic energy.

Upon entering the Earth's upper atmosphere, primary cosmic rays interact with atoms that constitute the air and they undergo nuclear reactions which generate a cascade of different particles called secondary cosmic rays (figure 1.1). The most abundant particles emerging from these collisions are pions. In particular, charged pions quickly decay into muons which easily penetrate through the atmosphere and reach the surface of the Earth. This is possible because muons do not interact strongly with matter as pions do and, on the other hand, time dilation affects their mean lifetime which is about 2.2 μs at rest.

At sea level, muons are the most abundant compared to other particles of the air-shower. The average energy is comprised between 3 and 4 GeV and the flux is about 10000 $m^{-2}min^{-1}$, with a maximum value at the zenith and a dependency with respect to the muon momentum. Using a suggestive picture, it means that about one muon passes through the palm of your hand every second [1, 2, 3, 4].

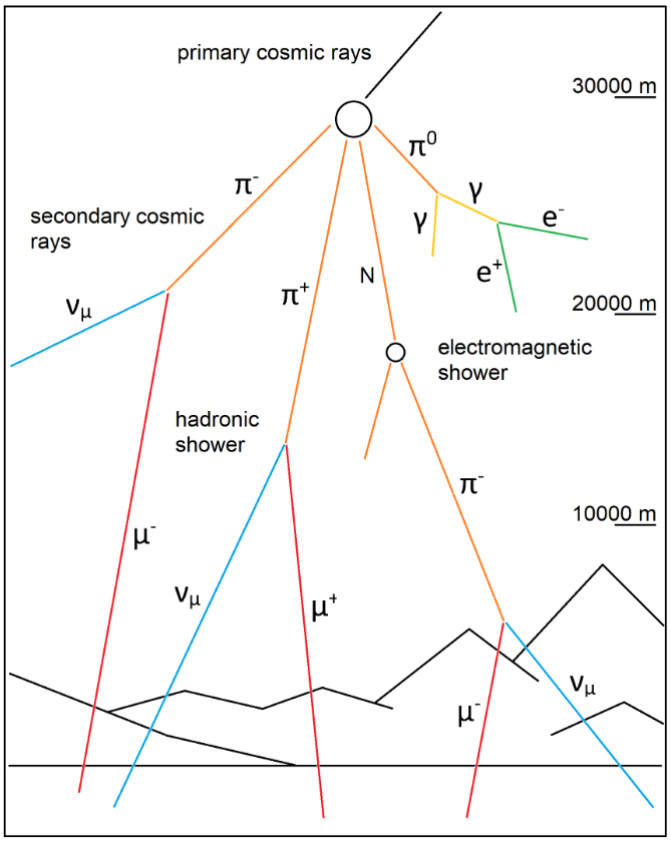

Figure 1.1: interaction of cosmic rays with the Earth's atmosphere.

When muons pass through a material, they lose energy through inelastic collisions with the atomic electrons. The average energy lost per unit length is expressed by the mass stopping power $\langle -\mathrm{d}E/\mathrm{d}X \rangle$, in units of $MeV\ g^{-1}cm^{-2}$, where $\mathrm{d}X$ corresponds to the product $\mathrm{d}x \cdot \rho$, being ρ the density of the material crossed in $g\ cm^{-3}$. The stopping power as a function of $\beta\gamma = p/Mc$, where p and M are correspondingly the momentum and mass of the muon, is well-described by the Bethe-Bloch formula in the range $1 < \beta\gamma < 1000$ (figure 1.2):

$$\left\langle -\frac{\mathrm{d}E}{\mathrm{d}X} \right\rangle = Kz^2 \frac{Z}{A} \frac{1}{\beta^2} \left[\frac{1}{2} \ln \frac{2m_e c^2 \beta^2 \gamma^2 W_{max}}{I^2} - \beta^2 - \frac{\delta(\beta\gamma)}{2} \right] \tag{1.1.1}$$

where K is a proportionality coefficient, z the charge number of the muon, A and Z the mass and atomic number of the crossed material, I the mean excitation potential, m_e the mass of the electron, W_{max} the maximum energy transfer in a single collision and $\delta(\beta\gamma)$ the density effect correction to ionisation energy loss.

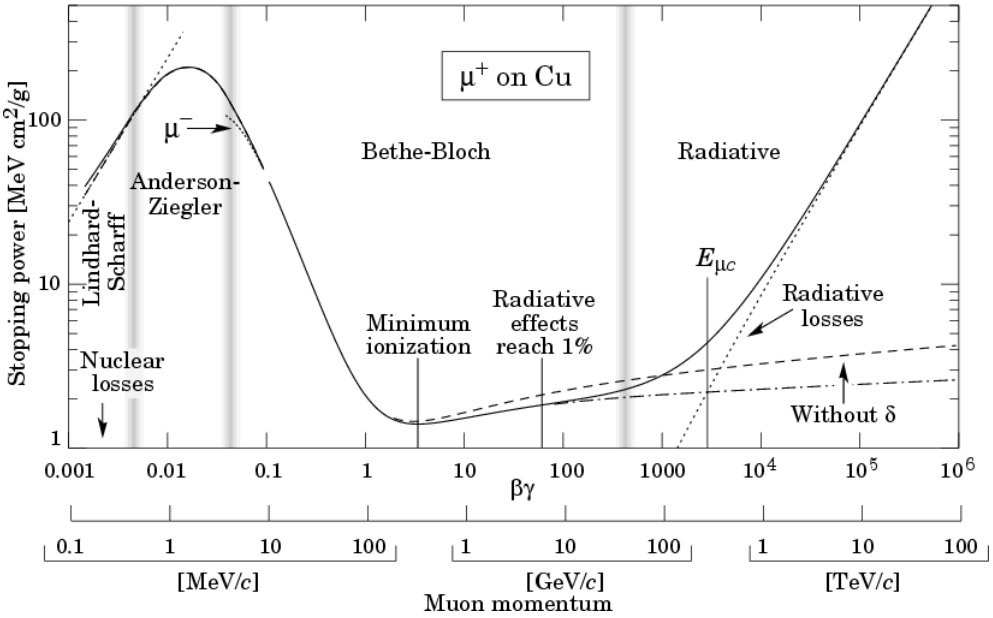

Figure 1.2: mass stopping power for positive muons in copper as a function of $\beta\gamma$ [1].

Another important process is the deflection of the incident direction of muons due to elastic scattering from nuclei of the crossed material, called Coulomb scattering. Depending on the thickness of the crossed material, the effect is referred to as single or multiple scattering (figure 1.3). In the latter case, the process can be treated statistically and the resulting distribution of scattering angles can be approximated by a gaussian (figure 1.4) with a root mean square given by the following equation:

$$\sigma_\theta = \frac{13.6\ MeV}{\beta cp} z \sqrt{\frac{x}{X_0}} \left[1 + 0.038 \ln\left(\frac{xz^2}{X_0 \beta^2} \right) \right] \tag{1.1.2}$$

where x is the thickness of the crossed material and X_0 is the material radiation length, described by:

$$X_0 = 716 g/cm^2 \frac{A}{Z(Z+1) \ln\left(\frac{287}{\sqrt{Z}}\right)} \tag{1.1.3}$$

For higher energy range, muons undergo other processes, such as the Cherenkov effect and bremsstrahlung, but their contribution can be neglected for the purposes of this thesis [1].

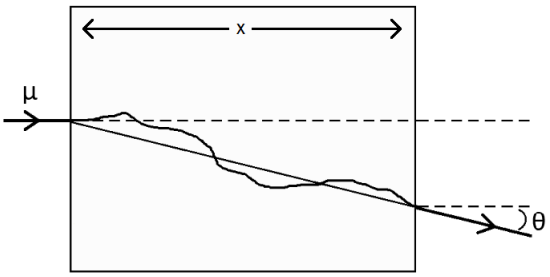

Figure 1.3: multiple Coulomb scattering.

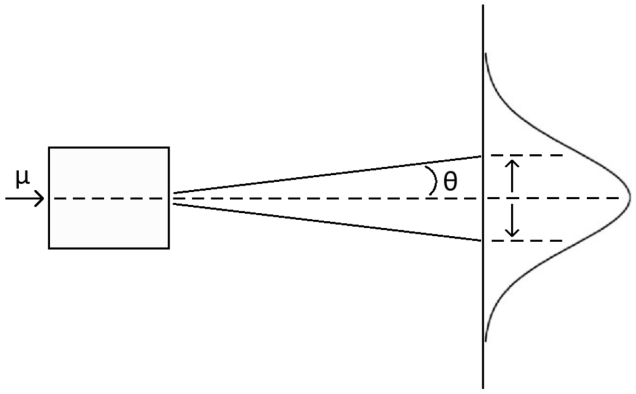

Figure 1.4: gaussian distribution of scattering angles.

1.2 Drift tubes

A muon detector can be made using gaseous detectors as drift chambers, also called drift tubes since the common shape is a cylindrical, earth-grounded metal tube with a coaxial anode wire connected to a high positive voltage (figure 1.5). The tube is filled with a gas mixture, usually argon with the addition of molecular gases such as CO_2 to quench gas discharges inside. When the charged muon crosses the tube, if it has enough energy it ionises the gas atoms along its path, producing positive ions and electrons. The ions move toward the cathode while electrons drift toward the anode and if the electric field is high enough they are amplified in an avalanche process. This charge multiplication induces a signal which is read-out by front end electronics. The electron drift velocity depends on the gas type and on the electric field and in general it is not constant. Combining several layers of drift tubes in the orthogonal direction provides knowledge of both coordinates with good spatial resolution by measuring the electron drift time [1, 5].

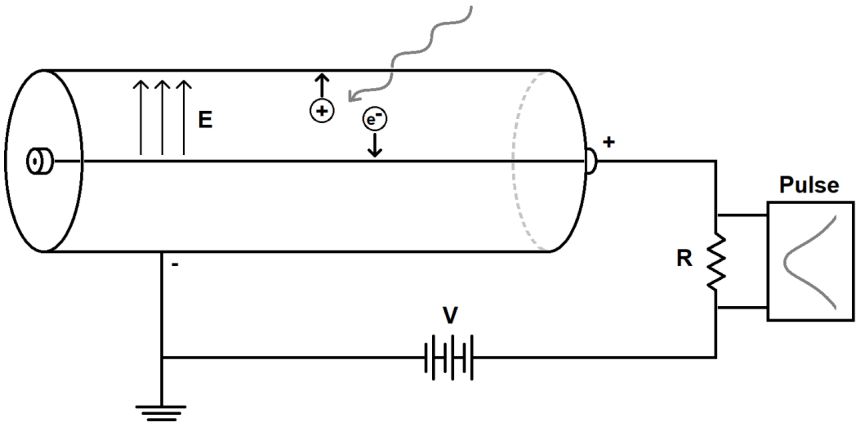

Figure 1.5: gaseous detector outline.

1.3 Muon tomography and applications

Muon tomography is a technique used to reconstruct a three-dimensional image of a given material using multiple Coulomb scattering (MSC) of muons. It requires the installation of detectors to measure both the incoming and outgoing trajectories of the muons in order to determine the scattering angles from which information on the density of the unknown material can be obtained. The presence of detectors on both sides of the volume also allows the MSC to be combined with information from muon absorption by measuring the attenuation of the intensity of their flux as they cross the material under analysis.

Muon tomography was first developed by scientists at Los Alamos National Laboratory in 2003 and since then more and more research groups have investigated many applications of this imaging technique. An important example is the inspection of dry storage casks (DSC) for spent nuclear fuel. Although safety protocols for transporting DSCs and storing them in spent fuel facilities are very reliable, during long storage times it is necessary to re-verify the contents, e.g. to contrast nuclear contraband which can lead to disastrous consequences. In fact, a DSC can contain up to 50 significant quantities (SQs), where a SQ indicates a quantity of nuclear material sufficient to produce a nuclear explosion. Muon tomography can be an effective re-verification method since it allows to detect or exclude the presence of spent fuel assemblies without opening the containers. Typical DPCs are CASTOR®-V casks with a mass of more than 120 t when fully loaded, a height of about 5 m and an external diameter of 2.4 m (figure 1.6) [1]. The Padova research group involved in muon tomography studies is committed to realize two detectors based on drift tubes that will be placed in proximity of a CASTOR®-V cask to prove the feasibility of this application.

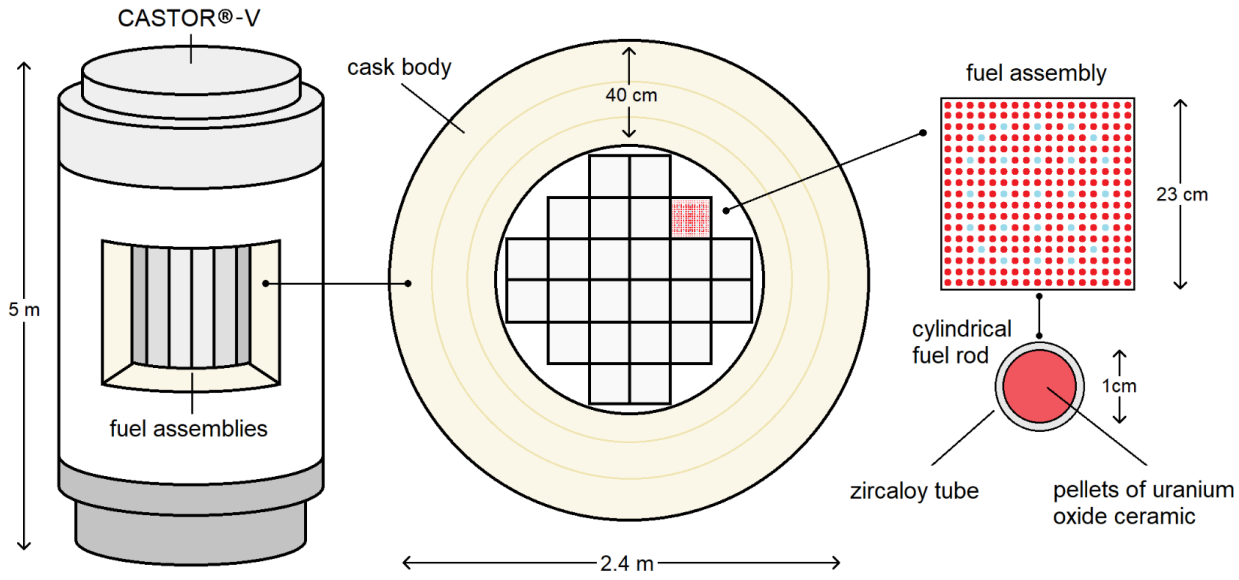

Figure 1.6: schematic view of a CASTOR ®-V cask and its cross section.

1.4 Objectives

The first objective of this thesis is to estimate the radial and longitudinal spatial resolution of a drift tube by taking as a reference the muon track reconstruction performed by the muon tomography demonstrator installed at Legnaro National Laboratories. The second objective is to determine the optimal position of CMS superlayers with respect to detectors, obtained by joining several layers of drift tubes of the type tested in this study, placed around a CASTOR®-V cask.

Experimental setup

The experimental setup for the first objective consists of a cylindrical drift tube 4 m long, with a diameter of 5 cm and a thickness of 1.5 mm (figure 2.1). Inside, there is a coaxial beryllium copper anode wire, 100 μm thick, maintained at a mechanical tension of about 6 N and electrically connected to a voltage of 3000 V which generates an electric field that goes as $1/r$, being r the radial distance from the wire. The drift tube is filled with an $Ar/CO_2 = 85\%/15\%$ gas mixture that flows inside the tube at a rate of 100 ml/s. The end of the drift tube is connected to the read-out electronics that measure the electrical pulses produced by the passage of muons that ionize the gas molecules. However, in this study the system has been modified to read signals from both ends which are referred to as "Front" and "Back".

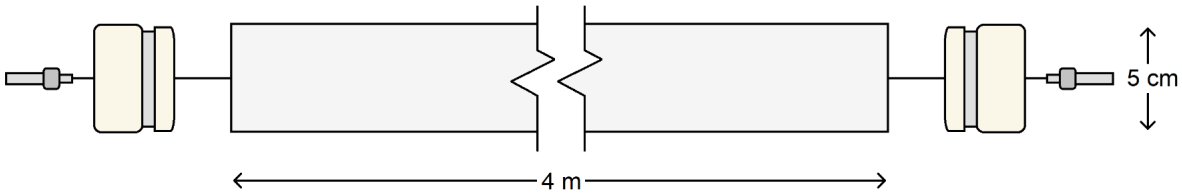

Figure 2.1: drift tube outline.

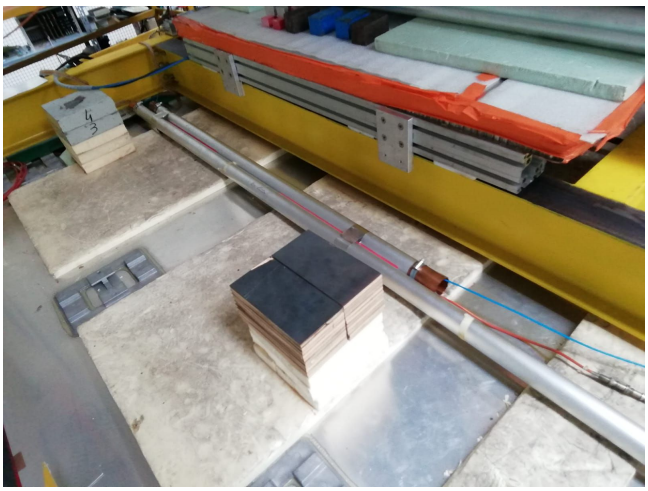

Figure 2.2: drift tube setup (the longer one in the picture).

The drift tube is placed in the muon tomography demonstrator installed at Legnaro National Laboratories, consisting of two CMS chambers, i.e. drift chambers used in the CMS experiment at CERN. The chambers are made of three independent superlayers, joined together and with a honeycomb plate, in each of which there are 4 layers of rectangular drift cells. In particular, the even layers are staggered by half a step in relation to the odd ones. Two superlayers measure the coordinate in the CMS bending plane and the third one measures the coordinate along the beam direction [6]. In this study the CMS chambers are used to reconstruct the passage of muons and to provide a trigger system for the drift tube under analysis. Therefore, they allow to derive the electron space-drift time relation inside the tube. The chosen frame of reference is shown in figure 2.3. Data are gathered with the request that muons pass through the upper CMS chamber and the reconstructed tracks point to the lower one. If muons pass through the drift tube they produce signals that are read from both sides of the tube. The event acquisition rate is about 340 Hz and the dataset used for this study consists of more than 4×10^6 events.

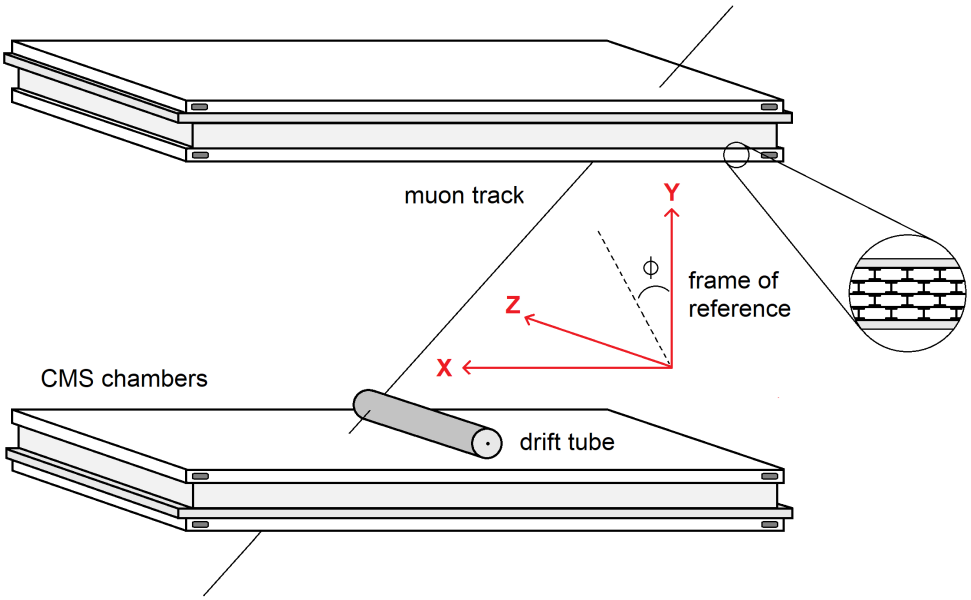

Figure 2.3: CMS chambers outline and frame of reference. Note that the size of the drift tube is not respected.

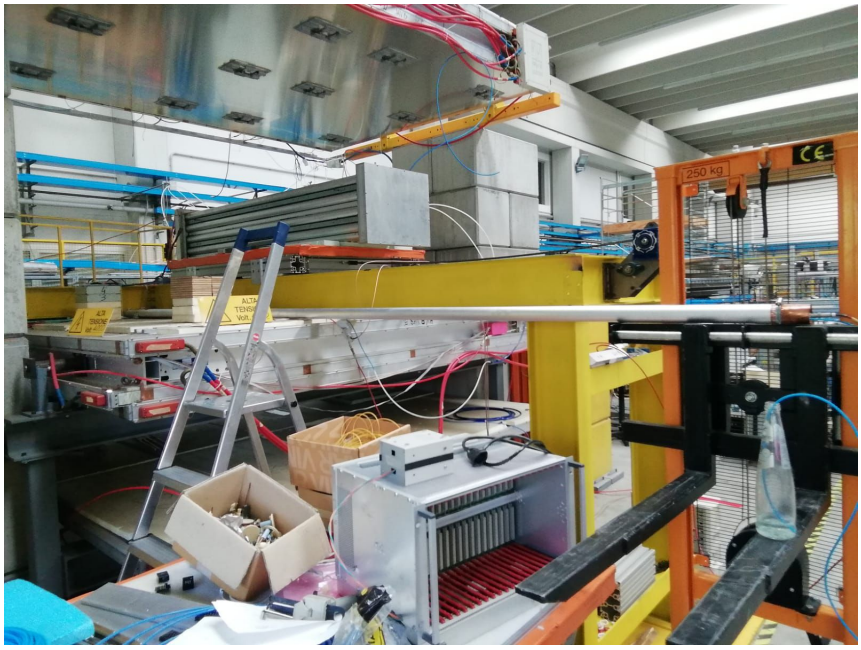

Figure 2.4: experimental setup at Legnaro National Laboratories. Above and below it is possible to see the CMS chambers while between them there are the 4 m drift tube and an additional detector not studied in this thesis.

The experimental setup for the second objective of this study consists of a detector obtained by joining togheter 6 layers of drift tubes of the the tybe described above (figure 2.5). Each layer is made of 30 or 31 tubes and it is staggered by half a step from the contiguous ones. This configuration allows the position of muon tracks in the xy plane to be reconstructed with very good resolution, while the longitudinal coordinate estimate is much worse (this result is discussed extensively for a single drift tube in section 3.2). For this reason, the drift tube detector is combined with a CMS superlayer placed orthogonally with respect to the direction of the tubes in order to reconstruct the z coordinate with good resolution as well. Note that the relative position between the detector and the CMS superlayer can be modified.

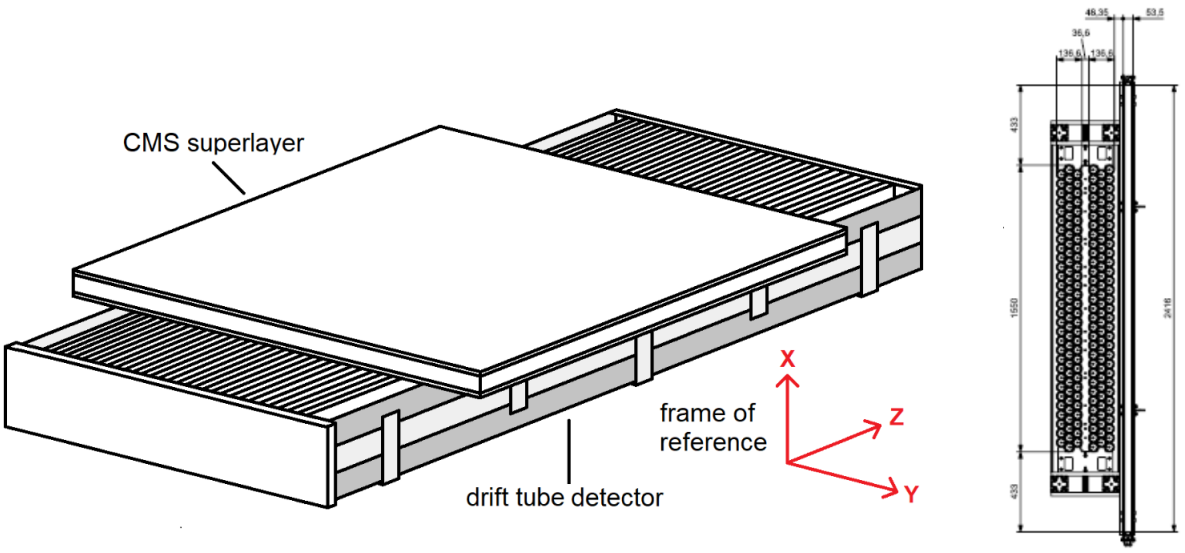

Figure 2.5: outline (on the left) and plan (on the right) of the drift tube detector with a CMS superlayer.

Two drift tube detectors joined to their CMS superlayers are positioned opposite each other around a CASTOR®-V cask, as can be seen from figure 2.6. The muon flux is simulated by a program using energy and angular spectrum information obtained from experimental data [7] while muon interactions with the crossed material are recreated by GEANT4, a toolkit for the simulation of the passage of particles through matter [8]. In particular, muons are generated by two different types of surfaces: either a 'flat sky' with an area of $15 \times 15\ m^2$ placed over the cask or a hollow cylinder of height $h = 5\ m$ containing it. Simulated events are accepted only if the muons originate from outside the drift tube detectors and point toward the cask.

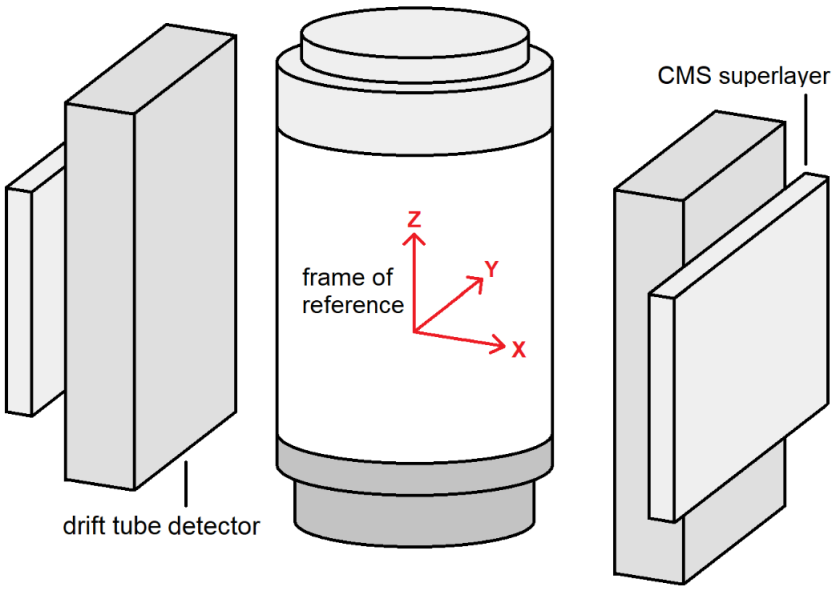

Figure 2.6: schematic view of the experimental setup.

Data analysis and discussion

3.1 Radial spatial resolution

The first step in estimating the radial spatial resolution of the drift tube is to determine its position in space with respect to the chosen frame of reference, i.e. calculate the so-called geometric parameters. After having measured the distance h between the two chambers and obtained a raw value of the height y_0 of the wire, it is possible to calculate the x, y and z coordinates of the muon passage with respect to the anode using those reconstructed by the CMS chambers, which are labeled with a subscript "ch".

The z coordinate, displayed on the zy plane, represents the projection on the z axis of the point identified by the intersection of the muon track and the anode initially assumed to be perfectly aligned with the z axis. Note that in figure 3.1, as in the following ones describing the geometry of the system, the sizes are not respected. In fact, looking at the histogram in figure 3.2, it can be seen that on the right-hand side the events end suddenly, as the corresponding side of the tube is completely contained by the CMS chambers, while on the left-hand side the slope is gentler as the drift tube actually protrudes from the chambers.

$$z = z_{ch2} + y_0 \frac{(z_{ch1} - z_{ch2})}{h} \tag{3.1.1}$$

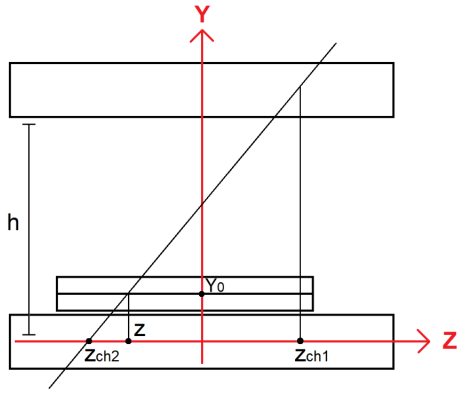

Figure 3.1: z coordinate geometry.

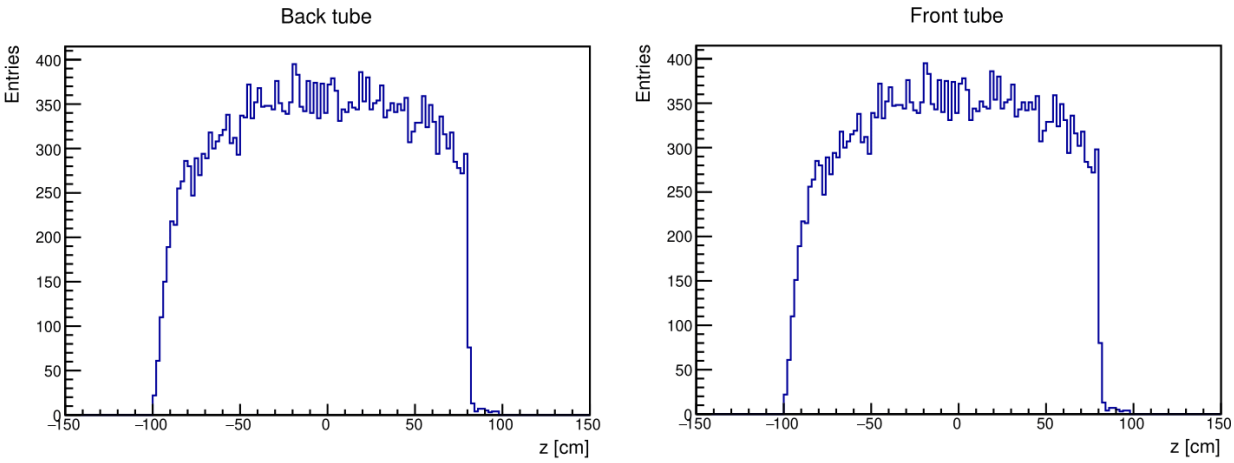

Figure 3.2: z coordinate of events with a signal on the Back side (left panel) and on the Front side (right panel).

The x coordinate, displayed on the xy plane, is the projection on the x-axis of the point identified by the intersection of the muon track with a straight line parallel to the x-axis passing through the anode while the parameter $corr_{yz}$ represents the correction which compensates for any non-alignment of the drift tube with respect to the ground and it is initially set to zero:

$$x = x_{ch2} + (y_0 + corr_{yz})\frac{(x_{ch1} - x_{ch2})}{h} \tag{3.1.2}$$

$$\tan\phi \equiv \frac{(x_{ch1} - x_{ch2})}{h} \tag{3.1.3}$$

$$corr_{yz} = z \cdot tilt_{yz} \tag{3.1.4}$$

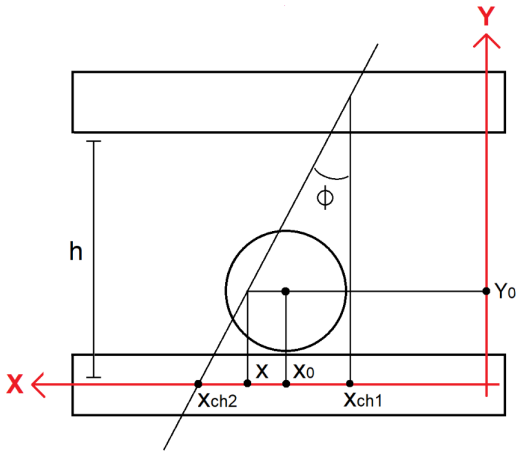

Figure 3.3: x coordinate geometry.

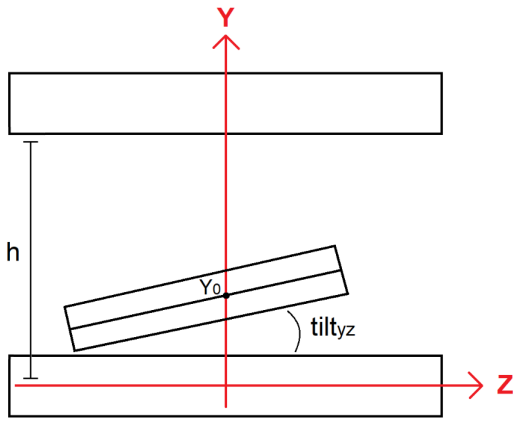

Figure 3.4: parameter $corr_{yz}$.

A first estimate of the anode position x_0 in the xy plane can be obtained by calculating the average value of the x coordinates of each event because their distribution is approximately uniform as it can be seen in figure 3.5:

$$x_0 = \frac{\sum_i^N x_i}{N} \tag{3.1.5}$$

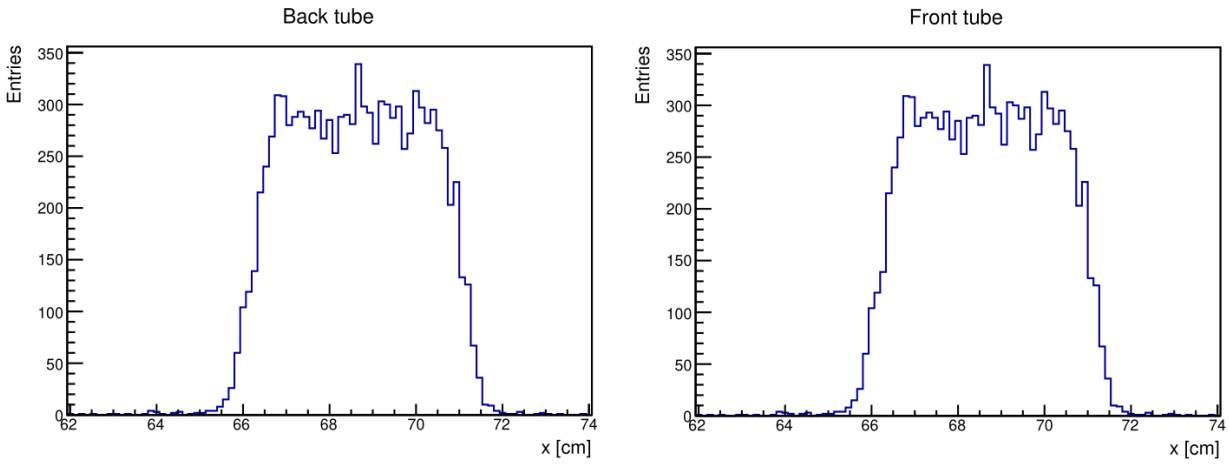

Figure 3.5: x coordinate of events with a signal on the Back side (left panel) and on the Front side (right panel).

The radial distance, reconstructed by the CMS chambers, is calculate as the minor distance between the muon track and the x_0 anode position corrected with a new parameter $corr_{xz}$, also initially set to zero, which rapresents a possible non-alignment of the anode wire with respect to the z-axis:

$$Dr = \frac{x - (x_0 + corr_{xz})}{\sqrt{1 + \tan^2 \phi}} \tag{3.1.6}$$

$$corr_{xz} = z \cdot tilt_{xz} \tag{3.1.7}$$

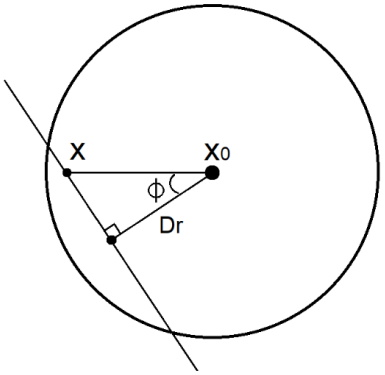

Figure 3.6: radial distance.

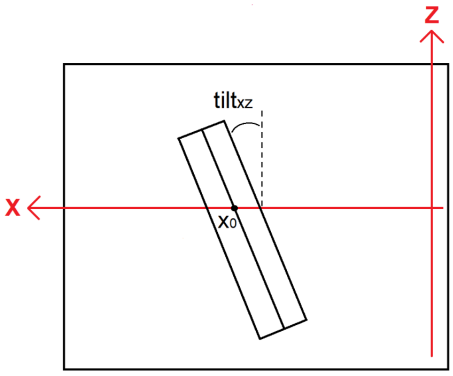

Figure 3.7: parameter $corr_{xz}$.

Finally, the y coordinate, displayed on the xy plane, is the projection on the y-axis of the point identified by the intersection of the muon track with a straight line parallel to the y-axis passing through the anode corrected by the parameter $corr_{xz}$:

$$y = \frac{(x_0 + corr_{xz}) - x_{ch2}}{\tan \phi} \tag{3.1.8}$$

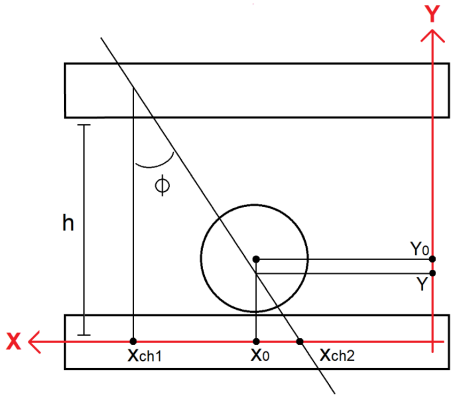

Figure 3.8: y coordinate geometry.

Since the radial distance depends on the z coordinate, as shown in equation 3.1.6, it is possible to construct a graph Dr vs. z, selecting only the events for which the muon passed near the anode. This condition is equivalent to operationally selecting events with a small drift time, measured by the drift tube, which also supposedly corresponds to a small radial distance. Figure 3.9 shows the histogram of drift times expressed in TDC counts, where 1 TDC count corresponds to $25/32\ ns$. Note that the histogram does not include the conversion of the unit of measurement due to display reasons. The data of the Dr vs. z graph (figure 3.10) are then interpolated with a straight line of equation $Dr = mz + q$ where m is the angular coefficient corresponding to the term $tilt_{xz}$ while q is a correction to the first estimate of x_0. This allows the value of the parameter $corr_{xz}$ and the position x_0 of the anode to be updated. The procedure is iterated until the angular coefficient m is of the order of $10^{-4}/10^{-5}$.

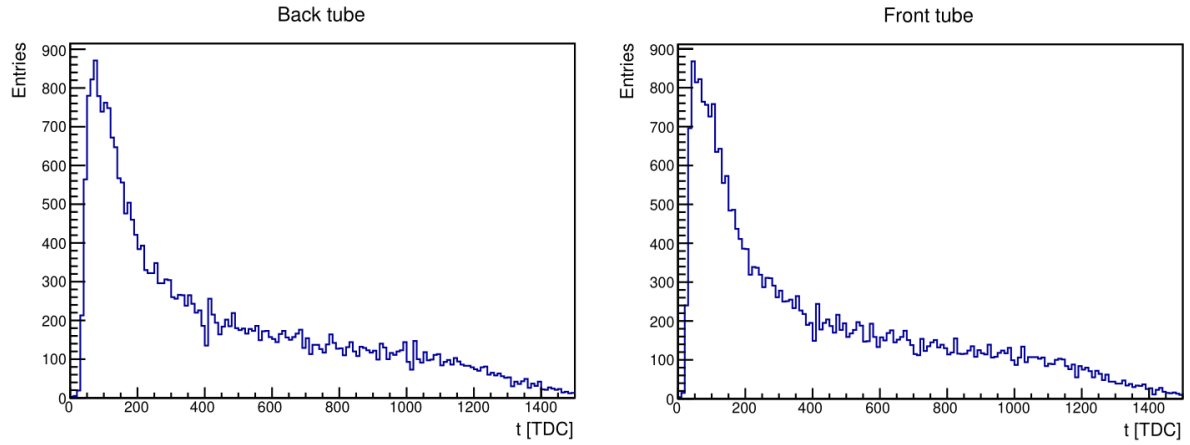

Figure 3.9: drift times.

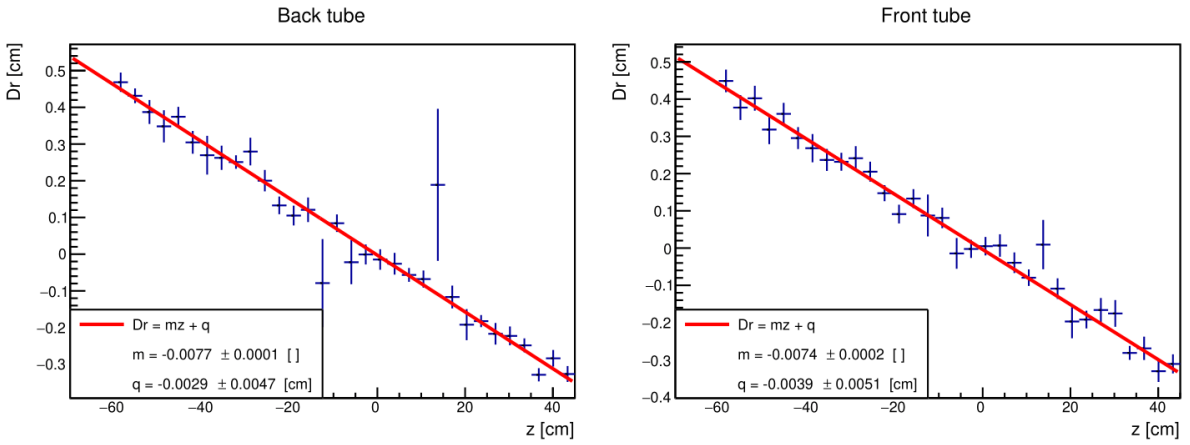

Figure 3.10: Dr vs. z, first iteration.

Similarly to what has been done for the graph Dr vs. z, it is possible to construct a graph y vs. z (figure 3.11) again selecting only the events for which the muon passed near the anode wire. The data are then interpolate with a straight line of equation $y = mz + q$ where m is the angular coefficient corresponding to the term $tilt_{yz}$ while q is an estimate for y_0. This procedure allows to obtain an estimate for the correction parameter $corr_{yz}$. The first and second procedures just described are iterated until the geometrical parameters improve further.

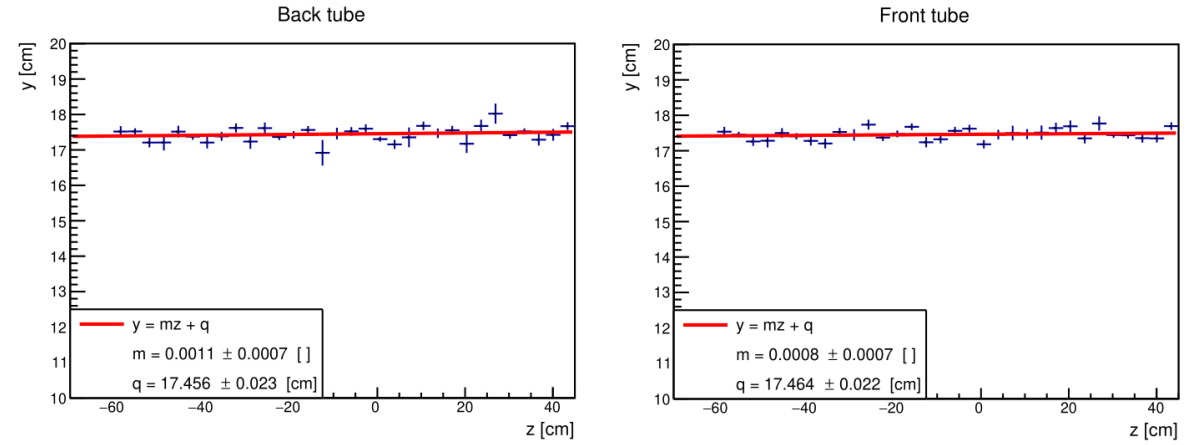

Figure 3.11: y vs. z, first iteration.

After having determined Dr with the updated geometrical parameters, it is possible to construct a space-time scatter plot (figure 3.12) that relates the radial distance as a function of drift time, expressed in TDC counts, measured by the drift tube using the CMS chambers as trigger system. This graph was then overlaid with a curve representing the radial distance $Dr_{tube}(t)$ reconstructed by the drift tube whose analytical form was derived over several years of study of this particular type of detector [9]. The parameters of the curve are obtained by fitting the data gathered distinguishing the Front signal from the Back one. As it can be seen from table 3.1, Front and Back parameters are very similar except the first one. This difference is related to the fact that the Back signal has to travel a longer path and for this reason it is shifted with respect to the Front signal. For the following analysis the parameters of the Front signal have been chosen also for the Back one with the exception of $p[0]$.

$$Dr_{tube}(t) = p[1] \cdot \left(1 - e^{-\frac{t-p[0]}{p[2]}} + p[3] \cdot (t - p[0]) + p[4] \cdot (t - p[0])^2\right) \tag{3.1.9}$$

fit parameter	Front value	Back value	unit of measurement
p[0]	$(4.04 \pm 0.05) \times 10^1$	$(2.82 \pm 0.06) \times 10^1$	[TDC]
p[1]	$(7.9 \pm 0.2) \times 10^{-1}$	$(7.8 \pm 0.2) \times 10^{-1}$	[cm]
p[2]	$(1.32 \pm 0.04) \times 10^2$	$(1.31 \pm 0.04)) \times 10^2$	[TDC]
p[3]	$(2.1 \pm 0.1) \times 10^{-3}$	$(0.21 \pm 0.01) \times 10^{-3}$	[TDC^{-1}]
p[4]	$(-4.4 \pm 0.4) \times 10^{-7}$	$(-4.5 \pm 0.5) \times 10^{-7}$	[TDC^{-2}]

Table 3.1: fit parameters.

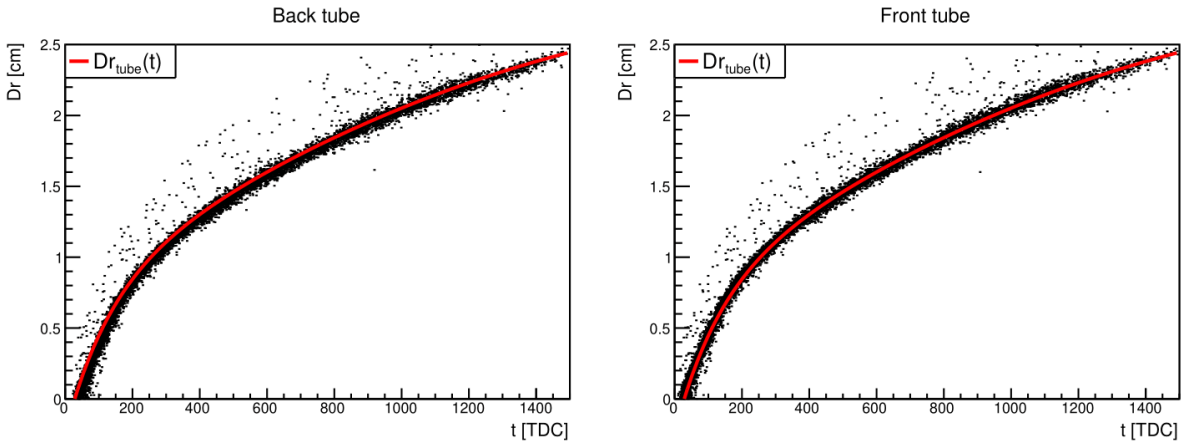

Figure 3.12: scatter plot Dr vs. t.

It is then possible to evaluate the resolution of the drift tube by plotting the difference between the radial distance reconstructed by the CMS chambers and the one reconstructed by the tube using equation 3.1.9. The data are then fitted by a gaussian curve whose deviation represents the convolution of the intrinsic radial spatial resolution of the drift tube and the extrapolation error, i.e. the error due to the CMS chambers measurement. In order to estimate the contribution of the latter, it can be noted that there are three different methods to measure the muon track. The first is to use only the upper CMS chamber, which gives the position of the muon in the plane of the chambers and its direction by means of the ϕ and θ angles. The second method uses the lower CMS chamber and is analogous to the first one, but in this case the extrapolation error is smaller, because the drift tube is located above the lower chamber. The third method is to plot the conjunction of the positions of the muon reconstructed from both CMS chambers and uses the geometric parameters of the tube. The first two methods provide independent measurements of the muon track, which could be used to derive an absolute estimate of the extrapolation error by constructing an instogram with their differences, but they are too different because the CMS chambers are spatially very far apart. On the other hand, the third method provides a measure that is correlated with both measures of the other two methods and therefore it is not possible to evaluate its error.

In order to estimate the contribution of the extrapolation error it would be necessary to have either an additional, much more accurate and independent measurement system or a redundant one, e.g. trough a track fit obtained by using a multilayer drift tube chamber observing that in such a case the interpolation error would be much smaller. Therefore, the events are operationally selected with the condition that at least two of the three measurement methods give the same result within about 100/200 μm, margin representing an estimate of the total error due to measurements from the CMS chambers. Looking at figure 3.13, it can be concluded that the radial spatial resolution of the drift tube is certainly less than about 300 μm and that the relative weight of the extrapolation error in the total convolution can be estimated in the order of 100/200 μm.

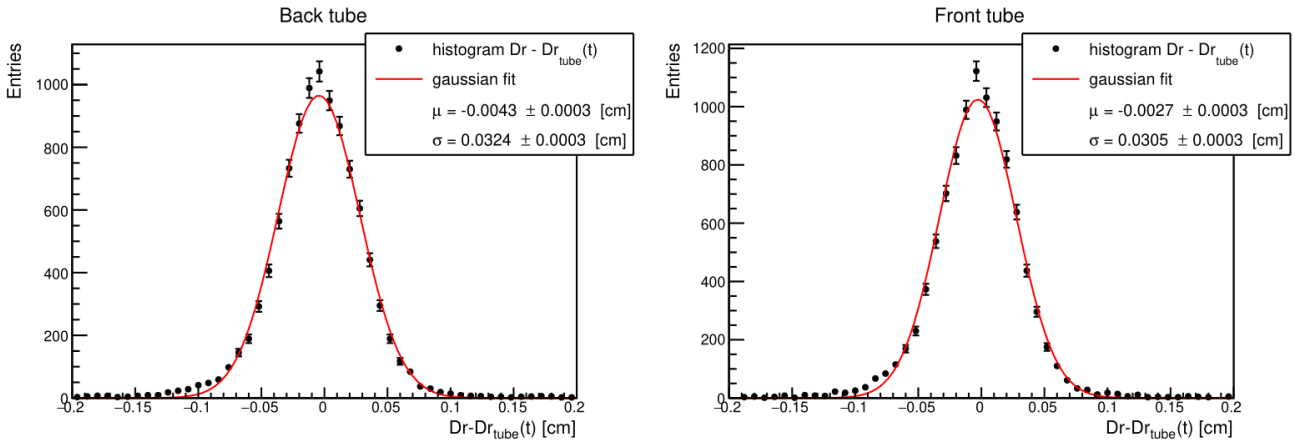

Figure 3.13: radial spatial resolution.

In order to subtract the contribution of the Back signal propagation along the part of the wire which protrudes from the CMS chambers, it is possible to calculate the mean drift time and re-evaluate the radial spatial resolution as a function of it. As can be seen from figure 3.14, the Back and Front times, referred to as tB and tF respectively, are highly correlated and this is due to the fact that the propagation time of the signal along the wire is much smaller than the drift time of the electrons.

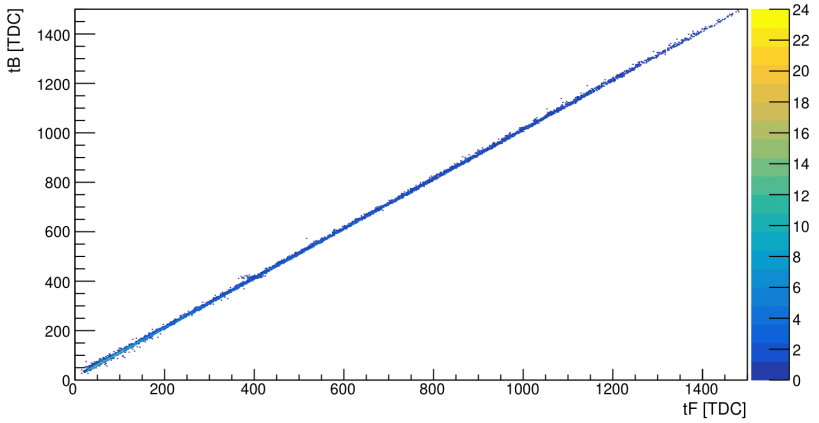

Figure 3.14: correlation between tB and tF.

It is then possible to construct a scatter plot of the radial distance Dr, reconstructed by the CMS chambers, as a function of the mean drift time $t\_mean = (tB + tF)/2$ and then overlay it with the 3.1.6 curve, whose parameters have been updated by means of a new data fit. As can be seen from table 3.2, the parameters $p[i]$ of the space-time curve are very similar to those obtained in the case where the Front and Back signals were kept distinct, except for the first one, which instead assumes an intermediate value. This result was predictable since the effect of considering the mean between the two signals, which have a linear dependence on each other, manifests itself in a rigid translation of the curve which is precisely described by the parameter $p[0]$.

fit parameter	value	unit of measurement
p[0]	$(3.43 \pm 0.05) \times 10^{1}$	[TDC]
p[1]	$(7.8 \pm 0.2) \times 10^{-1}$	[cm]
p[2]	$(1.30 \pm 0.04) \times 10^{2}$	[TDC]
p[3]	$(2.1 \pm 0.1) \times 10^{-3}$	[TDC^{-1}]
p[4]	$(-4.5 \pm 0.4) \times 10^{-7}$	[TDC^{-2}]

Table 3.2: fit parameters.

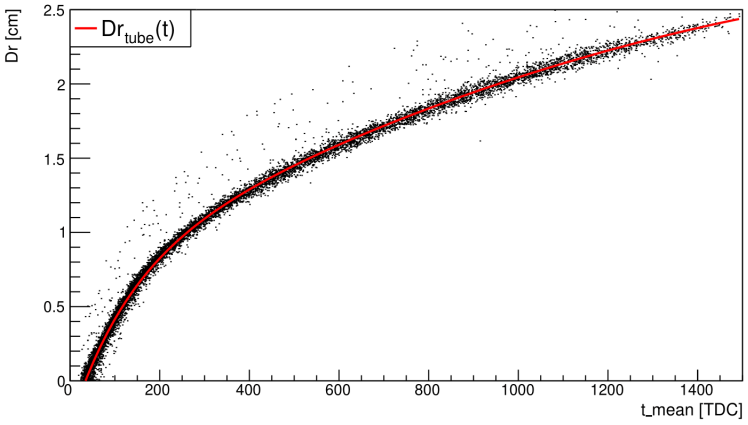

Figure 3.15: scatter plot Dr vs. t_mean.

Finally, the radial spatial resolution can be estimated by plotting a histogram of the differences between the two radial distances reconstructed by the CMS chambers and the drift tube and fitting the data with a gaussian curve (figure 3.16). The radial spatial resolution, represented by the deviation of the gaussian fit, has not changed significantly compared to the results obtained for the Front and Back signals. This result can be explained considering that the velocity propagation of the signal along the wire is much higher than the electron drift velocity in the tube. Consequently, the contribution given by the propagation time of the Back signal along the wire to the convolution with the electron drift time is negligible and the resulting resolution does not get worse, but neither it improves considerably.

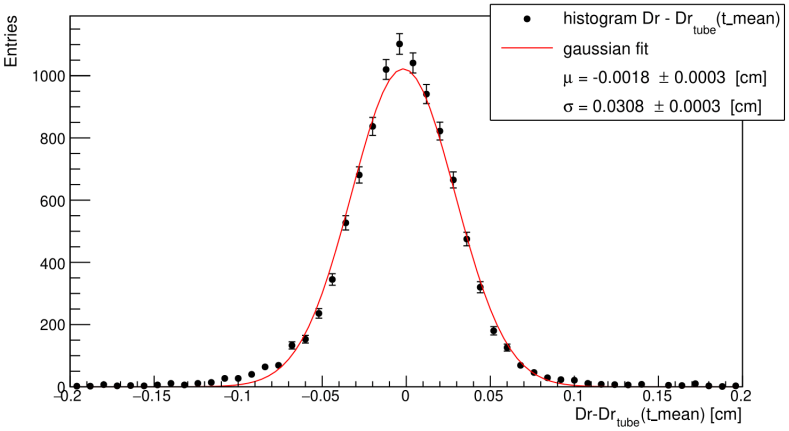

Figure 3.16: radial spatial resolution with t mean.

3.2 Longitudinal spatial resolution

Since the signal is read from both ends of the drift tube, it is possible to determine its longitudinal spatial resolution using the z-coordinate reconstructed by the CMS chambers. The first step is to estimate the velocity of propagation v_{tube} of the signal trough the anode wire, which can be treated as a coaxial cable. A reasonable approach is to construct a graph relating the time difference $\Delta t = tB - tF$ to the longitudinal coordinate z and interpolate the data with a straight line of equation $\Delta t = mz + q$ from which it is possible to estimate v_{tube} as the inverse of the angular coefficient. As can be seen from figure 3.19, the value obtained for the velocity of propagation, after converting TDC counts into seconds, is $v_{tube} = 1,64 \times 10^{10}\ cm/s$, which is 55% of the speed of light c.

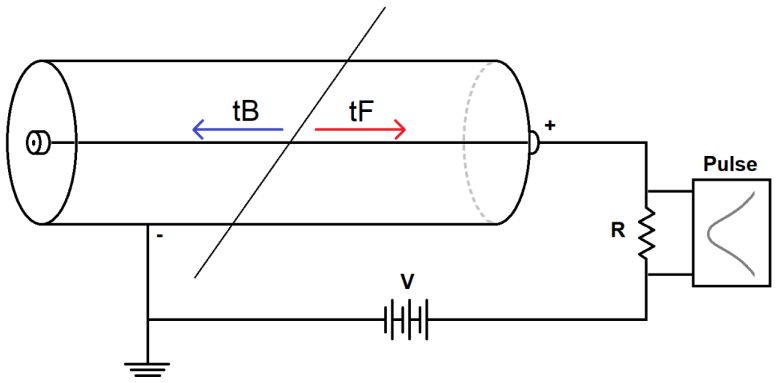

Figure 3.17: gaseous detector outline with double sided read-out system.

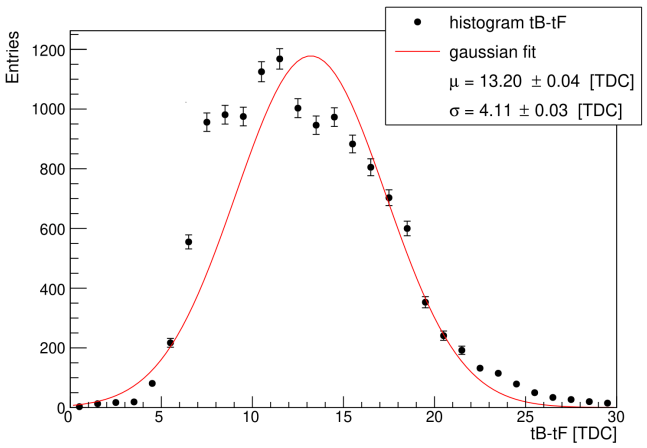

Figure 3.18: histogram tB-tF.

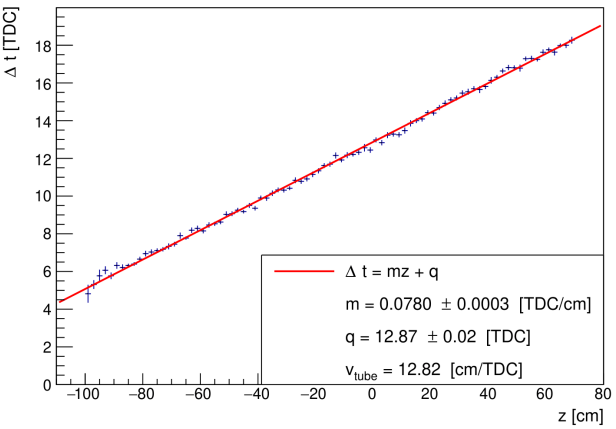

Figure 3.19: velocity of propagation.

The longitudinal coordinate z_{tube}, reconstructed by the drift tube, can be then calculated as the product of the velocity of propagation v_{tube} and the time difference Δt. As shown in figure 3.20, the resulting linear correlation between the two z-coordinate estimates is good. Finally, it is possible to construct a histogram of the differences $\Delta z = z_{tube} - z$ and fit the data with a gaussian curve whose deviation represents an estimate of the total longitudinal spatial resolution. Note that the gaussian fit has been done excluding the right tail of the histogram as there are edge effects disturbing the signal due to the fact that the longitudinal fluctuations, at the corresponding end of the drift tube, are reconstructed on one side only.

A possible solution to the problem would be to have larger CMS chambers in order to make more precise measurements and thus be able to exclude the tails on both sides of the tube. However, this demonstrates that it is possible to reconstruct the longitudinal coordinate of the muon track with a single drift tube even if the corresponding resolution is not optimal, as can been seen in figure 3.21.

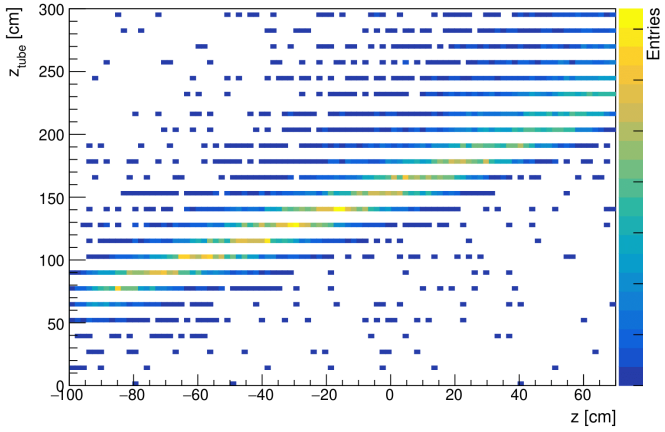

Figure 3.20: correlation between z_{tube} and z.

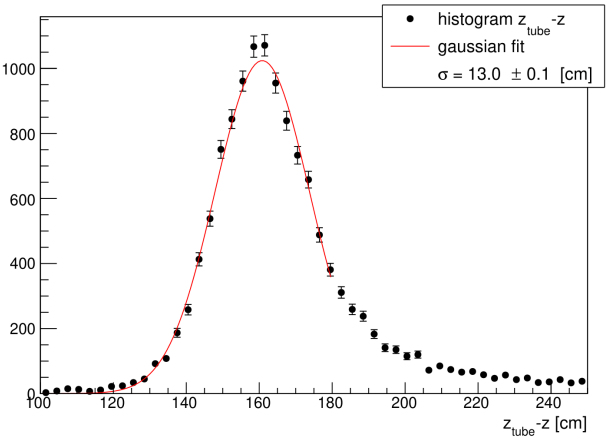

Figure 3.21: longitudinal spatial resolution.

3.3 Position optimisation for the CMS superlayers

In order to estimate the optimal position of the CMS superlayers (SL) with respect to the drift tube detectors, it is necessary to classify the simulated events into four categories. The first includes events such that the muons pass through a SL and the reconstructed tracks point to the opposite detector that actually measures the particle passage (figure 3.22a). The second includes events similar to the first, but in this case the muons are not measured by the other detector because they have been absorbed by the material (figure 3.22b). Events belonging to the first and second category are hereinafter referred to as 'SL good'. The third category is related to those events for which muons pass through a SL but the reconstructed tracks point to an area where the detection system is not present and, for this reason, they have been rejected in the analysis (figure 3.22c). Finally, the fourth category includes events with muons passing through the drift tube detector but not through the SL (figure 3.22d).

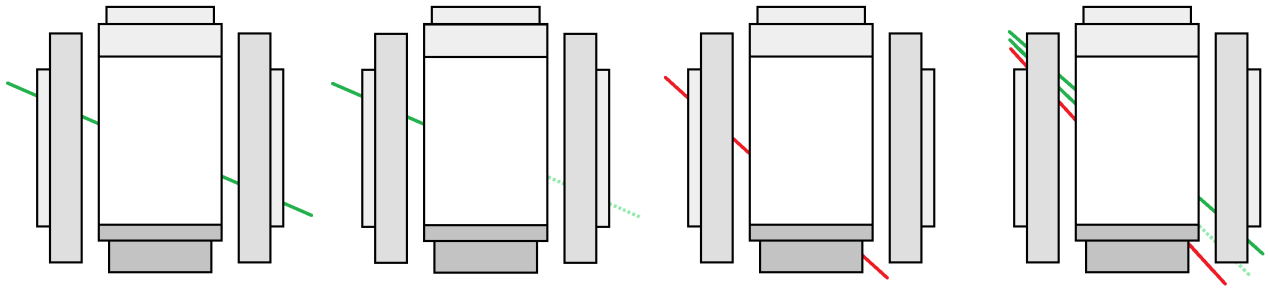

(a) (b) (c) (d)

Figure 3.22: simulated event categories.

Since the simulation allows the exact reconstruction of muon tracks for all listed categories, the idea is to change the height of the CMS superlayers so that the fraction of events belonging to the fourth category that actually point to the opposite drift tube detector is as small as possible because, in the experimental scenario, the low resolution on the longitudinal direction of the reconstructed tracks does not allow to distinguish muons that are absorbed from those pointing to the area without the detection system. The parameter used to estimate the optimal position of the SLs is given by the ratio between the 'SL good' events and the 'total good' ones that include both the 'SL good' events and those belonging to the fourth category pointing to the opposite detector.

Tables 3.3 and 3.4 show the values obtained when varying the height zSL of the CMS superlayers for both muon generating surfaces. As can be better seen from figure 3.23, in both cases the parameter improves as the height of the SLs increases. The values obtained with the two surfaces show significant differences. This can be due to the fact that the flat sky surface ($15 \times 15\ m^2$) can be not sufficient to simulate a large fraction of muon zenith angles. A larger surface can improve the angular distribution but would require a much larger event sample since the fraction of generated muons crossing the detectors decreases significantly. However, both generations show a similar tendency and therefore it can be concluded that it is convenient to place the CMS superlayers as high as possible with respect to the drift tube detectors.

total good	zSL [cm]	SL good	ratio $\pm\ \sigma_p$ [%]
966	110	379	39 ± 2
	130	464	48 ± 2
	150	571	59 ± 2
	170	694	71 ± 1
	190	801	82 ± 1
	210	910	94.2 ± 0.8

Table 3.3: flat sky-shaped muon generating surface.

total good	zSL [cm]	SL good	ratio $\pm\ \sigma_p$ [%]
1521	110	770	50 ± 1
	130	892	58 ± 1
	150	1022	67 ± 1
	170	1150	75 ± 1
	190	1276	83.9 ± 0.9
	210	1388	91.3 ± 0.7

Table 3.4: cylinder-shaped muon generating surface.

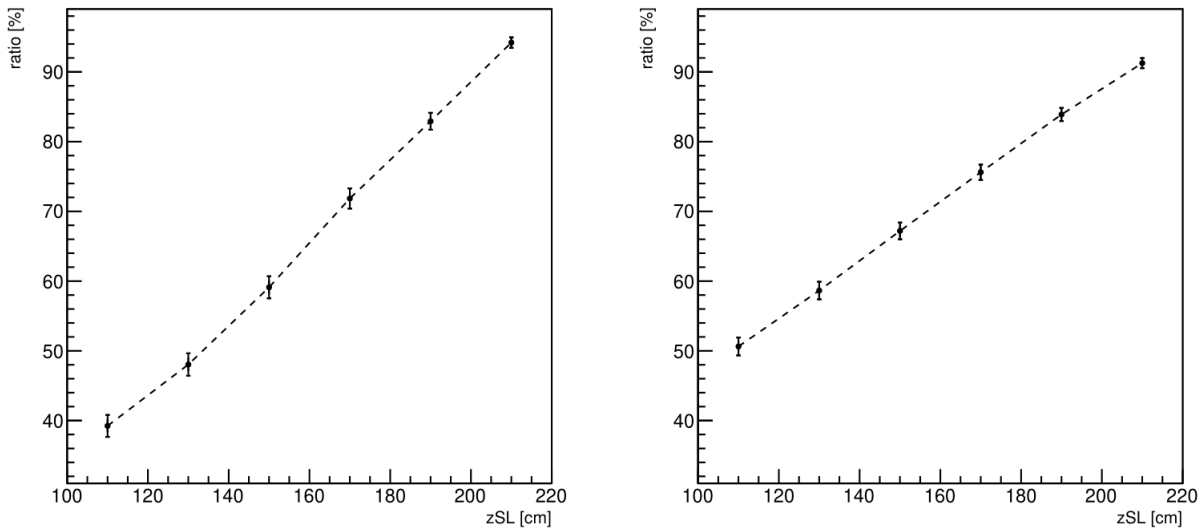

Figure 3.23: position optimisation for the CMS superlayers with flat sky-shaped (left panel) and cylinder-shaped (right panel) muon generating surfaces.

Conclusion

The study has shown that the radial spatial resolution of the drift tube is about 300 μm and the relative weight of the extrapolation error of the CMS chambers measurement has been estimated in the order of 100/200 μm. It has also been proved that it is possible to reconstruct the longitudinal coordinate of the muon track with a single drift tube by using a double sided read-out system. However, the longitudinal spatial resolution is not optimal as it is about 14 cm. Finally, regarding the position optimisation for the CMS superlayers, the results obtained from the simulation suggest to place the SLs as high as possible with respect to the drift tube detectors.

Bibliography

[1] G. Bonomi et al. "Applications of cosmic-ray muons". In: *Progress in Particle and Nuclear Physics* 112 (2020), p. 103768. ISSN: 0146-6410. DOI: https://doi.org/10.1016/j.ppnp.2020.103768. URL: http://www.sciencedirect.com/science/article/pii/S0146641020300156.

[2] Peter K.F. Grieder. "Chapter 1 - Cosmic Ray Properties, Relations and Definitions". In: *Cosmic Rays at Earth*. Ed. by Peter K.F. Grieder. Amsterdam: Elsevier, 2001, pp. 1–53. ISBN: 978-0-444-50710-5. DOI: https://doi.org/10.1016/B978-044450710-5/50003-8. URL: http://www.sciencedirect.com/science/article/pii/B9780444507105500038.

[3] Peter K.F. Grieder. "Chapter 2 - Cosmic Rays in the Atmosphere". In: *Cosmic Rays at Earth*. Ed. by Peter K.F. Grieder. Amsterdam: Elsevier, 2001, pp. 55–303. ISBN: 978-0-444-50710-5. DOI: https://doi.org/10.1016/B978-044450710-5/50004-X. URL: http://www.sciencedirect.com/science/article/pii/B978044450710550004X.

[4] Peter K.F. Grieder. "Chapter 3 - Cosmic Rays at Sea Level". In: *Cosmic Rays at Earth*. Ed. by Peter K.F. Grieder. Amsterdam: Elsevier, 2001, pp. 305–457. ISBN: 978-0-444-50710-5. DOI: https://doi.org/10.1016/B978-044450710-5/50005-1. URL: http://www.sciencedirect.com/science/article/pii/B9780444507105500051.

[5] H. Hilke and W. Riegler. "Gaseous Detectors". In: Sept. 2020, pp. 91–136. ISBN: 978-3-030-35317-9. DOI: 10.1007/978-3-030-35318-6_4.

[6] M Aguilar-Benítez et al. "Construction and test of the final CMS barrel drift tube muon chamber prototype". In: *Nucl. Instrum. Methods Phys. Res., A* 480.2-3 (2002), pp. 658–69. DOI: 10.1016/S0168-9002(01)01227-X. URL: http://cds.cern.ch/record/567321.

[7] L Bonechi. "Development of the ADAMO detector: test with cosmic rays at different zenith angles". In: (2005). URL: https://cds.cern.ch/record/965997.

[8] S. Agostinelli et al. "Geant4—a simulation toolkit". In: *Nuclear Instruments and Methods in Physics Research Section A: Accelerators, Spectrometers, Detectors and Associated Equipment* 506.3 (2003), pp. 250–303. ISSN: 0168-9002. DOI: https://doi.org/10.1016/S0168-9002(03)01368-8. URL: https://www.sciencedirect.com/science/article/pii/S0168900203013688.

[9] Paccagnella Andrea. "Costruzione e test di un rivelatore a muoni basato su tubi a deriva per misure in ambienti radioattivi". University of Padua, 2018.